Published in final edited form as:
Anal Biochem. 2012 August 15; 427(2): 164–174. doi:10.1016/j.ab.2012.05.019.

Fluorescence polarization assay for inhibitors of the kinase domain of receptor interacting protein 1

Jenny L. Maki[a,1], **Elizabeth E. Smith**[a,1], **Xin Teng**[b], **Soumya S. Ray**[c], **Gregory D. Cuny**[b,d], and **Alexei Degterev**[a,#]

[a]Department of Biochemistry, School of Medicine, Tufts University, Boston, MA 02111

[b]Laboratory for Drug Discovery in Neurodegeneration, Harvard NeuroDiscovery Center, Brigham & Women's Hospital and Harvard Medical School, Cambridge, MA 02139

[c]Center for Neurologic Diseases, Department of Neurology, Brigham & Women's Hospital and Harvard Medical School, Cambridge, MA 02139

Abstract

Necrotic cell death is prevalent in many different pathologic disease states and in traumatic injury. Necroptosis is a form of necrosis that stems from specific signaling pathways with the key regulator being RIP1, a serine/threonine kinase. Specific inhibitors of RIP1, termed necrostatins, are potent inhibitors of necroptosis. Necrostatins are structurally distinct from one another yet still possess the ability to inhibit RIP1 kinase activity. To further understand the differences in the binding of the various necrostatins to RIP1 and to develop a robust HTS assay, which can be used to identify new classes of RIP1 inhibitors, we synthesized fluorescein-derivatives of Necrostatin-1 (Nec-1) and Necrostatin-3 (Nec-3). These compounds were used to establish a fluorescence polarization (FP) assay to directly measure the binding of necrostatins to RIP1 kinase. The fluorescein-labeled compounds are well suited for HTS since the assays have a DMSO tolerance up to 5% and Z' scores of 0.62 (fluorescein-Nec-1) and 0.57 (fluorescein-Nec-3). Additionally, results obtained from the FP assays and ligand docking studies provide insights into the putative binding sites of Nec-1, Nec-3, and Nec-4.

Keywords

Necrostatins (Necs); Receptor Interaction Protein 1 (RIP1) kinase; fluorescence polarization (FP); competition assays; high-throughput screening (HTS); ligand docking

Introduction

Necrosis is a major component of pathologic tissue injury in ischemic brain and retinal damage, heart ischemia/reperfusion injury, intestinal inflammation and brain trauma [1,2].

[#]Corresponding author at: Department of Biochemistry, School of Medicine, Tufts University, Stearns 703, 136 Harrison Ave, Boston, MA 02111, USA. Fax: +1 617 636 2409, alexei.degterev@tufts.edu.
[d]Current Address: Department of Pharmacological and Pharmaceutical Sciences, 549A Science and Research Bldg 2, College of Pharmacy, University of Houston, Houston, TX 77204
[1]These authors contributed equally to this work.

The traditional view has been that necrosis is a nonspecific form of cell death caused by overwhelming stress. However, several recent studies have demonstrated that the activation of specific signaling pathways in the cell will result in cellular necrosis [3,4,5]. Programmed necrosis or necroptosis is a regulated caspase-independent form of cell death [6]. Necroptosis can be stimulated in a variety of cells by ligands (TNFα, Fas ligand, TRAIL) of death domain receptors when apoptosis is blocked or unavailable [7]. Although apoptosis and necrosis share similar activating stimuli, the outcome of the signaling is different forms of cell death [6]. The signaling mechanism of apoptosis has been well characterized but the mechanisms of necroptosis are just starting to be understood. Importantly, the kinase activity of receptor interacting protein 1 (RIP1) has emerged as a key inducer of necroptosis in a variety of in vitro and in vivo contexts.

RIP1 is a serine/threonine kinase that belongs to the RIP family of kinases. Two family members, RIP1 and RIP3, have been identified as components of TNF superfamily receptor signaling complexes and linked to the induction of necroptosis [8]. RIP1 consists of an N-terminal kinase domain, an intermediate domain, a RIP homotypic interaction motif (RHIM), and a C-terminal death domain [9]. In TNF-induced signaling RIP1 is recruited to the membrane-associated complex I and is K63 polyubiquitinated for NF-κB activation and cell survival. If cellular conditions are not optimal for survival, complex I releases RIP1 to form a cytosolic death-initiating signaling complex (DISC), which is also referred to as complex II. In addition to RIP1, complex II includes RIP3, TRADD, FADD, and caspase-8. In apoptotic signaling, caspase-8 may cleave de-ubiquitinase CYLD, RIP1 and RIP3, blocking initiation of necroptosis. However, if caspase-8 is inhibited then cells are trigged to undergo RIP1/RIP3 kinase-dependent necroptosis [6]. Although RIP1 is part of the complex in all three cell fates, NF-κB activation, apoptosis, and necroptosis, the kinase activity of RIP1 has been shown to be required primarily for TNF-induced necroptosis [10] and a limited number of specific instances of apoptotic death, i.e. induced by certain Toll-like receptor ligands and DNA damaging agents [11]. The kinase activity of RIP1 can be specifically inhibited by a series of small molecules termed necrostatins [10,12,13].

Necrostatins were discovered in a cell based screen to find inhibitors of death receptor mediated necroptosis. One of the hits from this screen was termed necrostatin-1 (Nec-1) [14]. This hydantoin-containing indole derivative (Figure 1, **1**) was optimized to yield a more potent inhibitor of necroptosis and RIP1 kinase activity (Figure 1, **3**) [15,16]. Two other structurally distinct inhibitor classes were also identified in the original screen [14], and then optimized resulting in a tricyclic derivative termed Nec-3 (Figure 1, **7**) [13] and [1,2,3]thiadiazole derivative Nec-4 (Figure 1, **9**) [12].

In this study, we synthesized two fluorescein-labeled necrostatins (Figure 2, **20** and Figure 3, **26**) for the development and optimization of a high-throughput fluorescence polarization (FP) assay for understanding the binding of different necrostatins to RIP1 kinase and for use in screening for new inhibitors. Both fluorescein-labeled necrostatins inhibit RIP1 kinase activity and demonstrate binding in the FP assay. We utilized competitions assays to determine the specificity of fluorescein-labeled compounds and in conjunction with ligand docking studies to understand the differences in binding modes between the structurally different necrostatins. Finally, the feasibility of these assays for HTS was tested with DMSO tolerance up to 5% and with Z' scores of 0.62 (fluorescein-Nec-1, Figure 2, **20**) and 0.57 (fluorescein-Nec-3, Figure 3, **26**). These assays are well suited for HTS enabling identification of novel inhibitors of RIP1 kinase as well as providing valuable tools for comparing modes of action of different necrostatins.

Materials and Methods

Reagents and chemicals

All chemicals and reagents were obtained from Sigma, Fisher, or VWR unless otherwise indicated.

Homology modeling and ligand docking

Induced fit docking: Glide 4.5 [17,18,19] was used for all docking calculations of both DLG-in and DLG-out structures of RIP1. Induced fit docking protocol with a softened-potential docking was performed to generate 20 initial poses. The softened-potential docking consisted of scaling the van der Waals radii by 0.5 except in the event when alanine substitutions were introduced, in which case the receptor scaling was set to 0.7. In this case Lys 24, Val 55 and Leu 136 were mutated to alanine to enhance the hit rate of poses in the initial docking that are close to the correct answer, the Glide hydrogen bond energy cutoff filter was decreased to −0.05 kcal/mol. This ensures that all retained poses contain at the very least a weak hydrogen bond with the receptor with backbone amide of Met 74. Second, the Glide Coulomb-vdW energy cutoff filter was increased to 10 kcal/mol, enabling toleration of more steric clashes than in a normal docking run. Poses with an RMSD of less than 0.5 Å and a maximum atomic displacement of less than 1.2 Å were eliminated as redundant in order to increase diversity in the retained ligand poses. An inner grid box of 10 Å was used to fit the ligand center and an outer box size of 20 Å was used.

For each of the top 20 poses (with respect to GlideScore) from the initial softened-potential docking step, a full cycle of protein refinement was performed. Prime uses the OPLS-AA parameter and a surface Generalized Born implicit solvent model. First, a list was generated consisting of all residues having at least one atom within 5 Å of an atom in any of the 20 ligand poses. All side chains in the list underwent a conformational search and minimization. Three residues that were mutated to alanine in the initial docking stage were returned to their original identity prior to the search. After convergence to a low-energy solution, an additional minimization was performed allowing all residues in the list (backbone and side chain) and the ligand to be relaxed. The complexes were ranked by Prime energy (molecular mechanics plus solvation) and those within 30 kcal/mol of the minimum energy structure were passed through for a final round of Glide docking and scoring.

The minimized ligand used in the first docking step is redocked using Glide with default settings into each of the 10 receptor structures produced in protein refinement step. A composite score that accounts for the protein/ligand interaction energy (GlideScore) [18,19] and the total energy of the system (Prime energy) is calculated using the following equation: (GlideScore) + (0.05 × PrimeEnergy).

The RIP1 kinase domain, between residues 17–285, was modeled using MODELLER [20,21,22]. Briefly, the main criteria in homology modeling were template selection and sequence alignment between the target and the template. The structure of Aurora kinase (>30% identity) was used for homology modeling since this enzyme has higher sequence conservation around the active site region to RIP1 than other kinases. The Cα RMSD and the backbone RMSD deviations for the model and the template crystal structure were < 1.0 Å and < 1.2 Å respectively. The best model was subjected to geometric evaluations using PROCHECK [23] with an overall G-value of −0.05. Ramachandran plots indicated that >93% of the residues are in the allowed region of the map [23,24]. Standard bond lengths and bond angles of the model were determined using WHAT IF [25] with an RMS-Z score of 0.8 and 0.9 suggesting that the model is of high quality [26].

The DLG-out conformation of the kinase was generated using PRIME [27] (Schrödinger Inc.). Briefly, loop conformation was sampled with the PRIME extended sampling settings. Side chains within 7.5Å of all residues remained flexible and all structures within a 50 kcal/mol energy window were saved. PRIME uses a hierarchal approach where the two major steps are dihedral angle sampling of the backbone to generate possible loop conformations (no steric clashes with other protein parts or inhibitors is ensured) followed by side-chain optimization of loop structures further chosen for optimization. The algorithm for side-chain optimization uses sampling from a highly detailed (10° resolution) rotamer library constructed by Xiang and Honig from a database of 297 proteins [28]. The final model was subject to MD thermalization to determine if it was a stable structure. In the thermalization scheme (simulated annealing), MD simulations of both the DLG-in and DLG-out out conformations of RIP1 described above were carried out using the DESMOND 3.0 (D.E Shaw Research and Schrödinger Inc.) [29,30] and the OPLS-AA 2005 force field [31]. Water solvation was described by immersion of the DLG-in (closed) and DLG-out (open) structures in 26,000 TIP3P waters. Electroneutrality was ensured by adding three Na+ ions to the system. Periodic boundary conditions and the particle mesh Ewald (PME) method (to account for long-range electrostatic interactions) were used throughout. Bonds involving hydrogens were constrained using the M-SHAKE algorithm and a time step integration of 2fs were used for all simulations. A steepest-descent minimization and thermalization scheme was applied to all of the initial structures. The systems were heated from 0 to 300 K in 200ps, keeping the Cα atoms fixed in their original positions. In the next step, all of the constraints were lifted, and the equilibration was continued in the isobaric–isothermal ensemble with Nose–Hoover thermostats for 1.0 ns.

Docking of Nec-1, Nec-3 and Nec-4 was performed using GLIDE v2.2 (Schrödinger Inc.) [17,18,19]. A 10Å search grid was used using the center of mass of P-loop and the activation loop as the point of origin. A hydrogen bond constraint was placed on backbone amide of M95. This reduced random conformation search significantly while docking. GLIDE docking was carried out in standard precision (SP) mode and at least 10 poses were requested with a docking score cutoff of −7.0 (anything lower than −7.0 was treated as a hit). The poses were inspected in Maestro 9.2 and selected for further analysis.

Synthesis of Nec-1 benzyl substituted analogs

Compound **10** was made according to our previous publication [15] by regioselective alkylation of the hydantoin with various benzyl bromides under basic conditions (Figure 2A).

Cellular EC_{50} determination of necrostatins

EC_{50} values of **Rac-3, 4, 5, 6,** and **7** were determined using CellTiter-Glo (Promega) luminescent cell viability assay as previously described [15,16].

Plasmid construction of GST-RIP1 kinase domain

The human RIP1 kinase domain (aa 8–327) was amplified by PCR using Phusion High-Fidelity Polymerase (New England Biolabs), digested with EcoRI and PstI restriction enzymes (New England Biolabs), and ligated into the same sites in the pAcGHLT-A Baculovirus Transfer Vector (BD Biosciences) creating the pAcGHLT-A-GST-hRIP1 8–327 plasmid. DNA sequencing (Core Facility, Tufts University) verified the correct sequence of the plasmid.

Protein expression and purification GST-RIP1 kinase domain fusion

Spodoptera frugiperda (Sf9) insect cells were grown in Sf-900 II SFM medium (Gibco/Invitrogen) at 27°C. To generate the GST-RIP1 baculovirus, 2 μg of pAcGHLT-A-GST-hRIP1 8–327 and 0.5 μg of linearized BaculoGold Bright DNA (BD Biosciences) were transfected into Sf9 cells using the BD BaculoGold Transfection Buffer A & B Set (BD Biosciences) according to the manufacturer's protocol and virus was amplified to passage four. For protein expression, Sf9 cells were grown in ESF921 Protein Free medium (Expression Systems) by shaking (150 rpm/min) at 27°C to a density of 3×10^6 cells/ml and infected with passage four baculovirus to express GST-hRIP1 8–327 recombinant protein. Five days after infection the cells were harvested and resuspended in lysis buffer (40 mM HEPES pH 7.3, 150 mM NaCl, 5 mM EDTA, 0.5 mM NaF, 0.2 mM NaVO3, 10 mM sodium pyrophosphate, 17.5 mM β-glycerolphosphate, 1 μg/ml aprotonin, 1 μg/ml leupeptin, 1 μg/ml pepstatin, 50 μg/ml PMSF). Cells were disrupted using a sonicator followed by centrifugation. Protein was purified using a 5 ml Glutathione 4B sepharose (GE Healthcare) column. GST-RIP1 fractions were combined, concentrated to ~1 ml, and injected onto a Superdex 200 10/300 GL Column (GE Healthcare Life Sciences). The protein was eluted using an isocratic gradient (50 mM Tris pH 8.0, 150 mM NaCl, 2 mM β-mercaptoethanol) for 1.5 column volumes and pure GST-RIP1 fractions were pooled and concentrated. Both 20% glycerol and 1 mM PMSF were added to the protein followed by flash freezing and storage at −80°C. The final protein concentration was determined using a NanoDrop 2000 Spectrophotometer (Thermo Scientific).

Radiometric Gel Kinase Assay

The assay was performed as described [10] with minor modifications. In kinase buffer (20 mM HEPES pH 7.3, 10 mM $MnCl_2$, 10 mM $MgCl_2$) 2 μM GST-RIP1 protein was preincubated with various concentrations of compounds for 10 minutes. Stock compounds in DMSO were further diluted with DMSO to the appropriate concentration and added to the reaction for a final DMSO concentration of 3% in all samples. The kinase reaction was initiated with the addition of 30 μM cold ATP and 3 μCi of [γ-^{32}P] ATP (Perkin Elmer) and incubated at 30°C for 30 min shaking at 600 rpm. Reaction were quenched by the addition of SDS-PAGE sample buffer and immediately boiled. The samples were run on a 15% SDS-PAGE gel and dried. Autophosphorylation of GST-RIP1 was visualized by gel exposure to x-ray film.

Synthesis of fluorescien-labeled necrostatins

The fluorescein analog of Nec-1 was prepared using the methodology outlined in Figure 2E. Phenol **12** was converted to triflate **13**, which in the presence of a Pd catalyst and zinc cyanide was transformed into **14** [32]. Bromination of this material gave **15** [33] 7-Chloroindole (**16**) was converted to **17a** and then to **17b** [34]. The nitrile was subsequently reduced to aldehyde **17c**, which was transformed to hydantoin **18** [15]. Regioselective alkylation of **18** with **15** gave **6**. Reduction of this nitrile generated **19**, which in the presence of FITC yielded the fluorescein-labeled Nec-1 derivative **20**. The final compound was verified by ^{1}H NMR (Supplemental Materials and Methods).

The fluorescein analog of Nec-3 was prepared using the methodology outlined in Figure 3A. Condensation of **21** and **22** give the chalcone **23**. Cyclization in the presence of hydrazine followed by acylation provided **24** (and its diastereomer, which was readily separated). Ester hydrolysis followed by HBTU-mediated coupling of N-Boc piperazine gave **25**. This material was de-protected with trifluoroacetic acid (TFA) and the resulting amine was coupled with FITC to give the fluorescein-labeled Nec-3 derivative **26**. The final compound was verified by ^{1}H NMR (Supplemental Materials and Methods).

General FP Methods

All FP experiments were conducted in 384-well, low volume, non-treated, round bottom, black polystyrene microplates (Corning 3677) and read using a Victor^{3}V 1420 Multilabel Counter (PerkinElmer). Polarization values are reported in millipolarization units (mP) and were determined using an excitation wavelength of 485 nm (15 nm bandwidth) and an emission wavelength of 535 nm (25 nm bandwidth) with a count time of 1 sec and a G-factor of 1.4.

Estimation of K_D values of fluorescent necrostatins binding to GST-RIP1 kinase domain

To each well was added: 1 μl of 750 nM **20** (50 mM Tris pH 8.0, 20% glycerol, 5 mM $MgCl_2$, 5 mM $MnCl_2$), 12.15 μl of increasing concentration (0 to 100 μM) of GST-RIP1 (50 mM Tris pH 8.0, 150 mM NaCl, 20% glycerol), 1.35 μl of 5X kinase buffer (100 mM HEPES pH 7.3, 50 mM $MgCl_2$, 50 mM $MnCl_2$), and 0.5 μl of DMSO. FP measurements were taken after a 10-minute incubation. The K_D of **20** was calculated using nonlinear regression one-site binding model (GraphPad Prism 5). The same procedure was used to calculate the K_D of **26**.

Estimation of IC_{50} and K_i values for unlabeled necrostatins

To each well, 50 nM of **20** was added to 2.6 μM of GST-RIP1 kinase domain and incubated for 5 minutes. Increasing concentrations of unlabeled compounds (0 to 100 μM) were added to the reaction with a final DMSO concentration of 3%. FP measurements were taken after a 10-minute incubation. The IC_{50} values were determined using nonlinear, variable slope fitting (GraphPad Prism 5). The K_i values were determined using the equation described by Nikolovska-Coleska et al. [35]. The same procedure was used with 50 nM of **26** and to 3.4 μM of GST-RIP1 kinase domain to calculate the IC_{50} and K_i values.

DMSO tolerance

Increasing concentrations of DMSO, 0–10% of the assay volume, were used to measure mP of **20** and mP of **20** with 2.6 μM of GST-RIP1. FP measurements were taken after 10-minute incubation. The same procedure was used with **26** and **26** with 3.4 μM of GST-RIP1 kinase domain.

Z' determination

To verify the assay for high throughput screening, the Z factor was calculated using the following equation: $Z'=1-((3\sigma_p + 3\sigma_n)/|\mu_p - \mu_n|)$ which was initially described in Zhang et al. [36]. σ_p and σ_n are the standard deviations of GST-RIP1/**20** and GST-RIP1/**20**/**Rac-3** respectively; whereas μ_p and μ_n are the averages. The following concentrations were used: 2.6 μM GST-RIP1, 50 nM **20**, and 50 μM **Rac-3**. Three independent experiments for each were combined and averaged. The procedure was used for 50 nM **26**, 3.4 μM GST-RIP1 and 50 μM **7**.

Result and Discussion

Development of fluorescein-labeled necrostatins

Our previous work revealed that the structurally dissimilar necrostatins, Nec-1, Nec-3 and Nec-4, (Figure 1A, **1**, **7**, **9**) all specifically target RIP1 kinase activity at sub-micromolar concentrations [10] and remain the only reported inhibitors of this kinase. Surprisingly, our previous data also suggests that each distinct necrostatin may have a different mode of RIP1 inhibition [10,13]. Given the emerging importance of necroptosis in numerous pathologic injuries and the widespread use of necrostatins to dissect the role of RIP1 kinase in vitro

[37,38,39,40] and in vivo [41,42,43,44,45,46], a better understanding of necrostatins' mode of action is critical for therapeutic development as well as in the identification of new classes of RIP1 inhibitors. In particular, new assays to directly measure the binding of structurally distinct necrostatins to RIP1 kinase will help guide new inhibitor development.

In our previous study using a cell-based necroptosis assay [15], we discovered that Nec-1 (Figure 1A, **1**) inhibitory activity was intolerant to substitution at several positions on the indole ring as well as many positions on the hydantoin ring. Despite the sensitivity to structural modification, the structure-activity relationship (SAR) study on Nec-1 enabled us to make an optimized version (**3**) but further modifications proved difficult. We re-examined the molecular model of RIP1/Nec-1 complex [10] using induced fit ligand docking to determine if Nec-1 preferentially bound the DLG-out or DLG-in conformation of RIP1. As our previous work suggested [10], Nec-1 interacted better with the DLG-out conformation. Therefore, we used this information to help guide the synthesis of a fluorescein-Nec-1 analog. According to our model (Figure 1B), the methyl group of hydantoin is positioned between the hinge and the N-terminal region of RIP1. The SAR study [15] demonstrated that replacement of the methyl on the hydantoin with an isopropyl group was not tolerated. This can be explained in the RIP1 molecular model by steric clashes between isopropyl and the side chains of L23 in the P-loop and various residues in the hinge, which are approximately 4–5 Å away from the carbon of the methyl group. However, the addition of a longer linker could allow for further modification to this position on the hydantoin.

To help determine if the addition of a longer linker attached to bulky hydrophobic fluorescein isothiourea group onto a N-benzyl substituted Nec-1 (i.e. Figure 2E, **20**) would potentially have an impact on binding to RIP1, we used the induced fit docking model of Nec-1 with fluorescein attached (Figure 1C, S1). In this model, the Nec-1 portion of **20** is making extensive contacts inside of the ATP binding pocket, while the addition of the a N-benzyl substituted linker projects the fluorescein group outside of the binding pocket and into the solvent making few if any molecular contacts with RIP1.

Using the docking study as a guide, we first synthesized Nec-1 intermediate analogs with various benzyl substituents on the hydantoin ring (**4**, **5**, **6**, and Figure 2A) to determine if a longer linker would retain inhibitory activity. These intermediate analogs were tested in a necroptosis cell viability assay (Figure 2B) as well as in a radiometric in-vitro kinase assay using recombinant GST-RIP1 (Figure 2C). Optimized racemic Nec-1 (**Rac-3**) has an EC_{50} of 180 nM in the cell-based necroptosis assay, while the addition of the benzyl on the hydantoin ring (**4**) caused an increase in the EC_{50} value to 748 nM. The chloro (**5**) and chloro/cyano (**6**) substitutions have only a slight difference in EC_{50} values, 220 nM and 420 nM respectively, from **Rac-3** (Figure 2B). The in-vitro kinase assay demonstrated that all of the inhibitors decreased the autophosphorylation of GST-RIP1 with the benzyl substituted compounds, **4**, **5**, and **6**, having a slight decrease in potency when compared to **Rac-3** (Figure 2C). These results suggest that addition of a benzyl group to the imide nitrogen of the hydantoin ring retains significant activity and provides a new direction for further Nec-1 derivatization.

Since our docking model suggested that addition of fluorescein to the benzyl linker would not significantly impact binding, we developed a method to synthesize a fluorescein-Nec-1 analog (**20**, Figure 2E). This compound was tested in the in-vitro kinase assay and inhibited the autophosphorylation of GST-RIP1 comparable to **Rac-3**, while the inactive Nec-1 analog **2** did not inhibit activity (Figure 2D). Compound **20** displayed an excitation maximum at 490 nm and an emission maximum at 515 nm, consistent with the spectrum of fluorescein. The values of perpendicular and parallel fluorescence of **20** substantially exceeded the background of buffer alone under the assay conditions (Figure S2). Therefore,

even though our previous data suggested a very restricted SAR of Nec-1[15], modification of the hydantoin nitrogen allowed us to successfully synthesize a fluorescent Nec-1 analog that retained inhibitory potency and possessed fluorescent properties needed for FP assay.

In addition to the synthesis of fluorescent Nec-1 analog **20**, we also attempted to develop a fluorescein-labeled analog of Nec-3, **7**. Using our previous SAR data for this compound series [13], we added a piperazine containing linker at the N1-position terminating in a fluorescein group resulting in compound **26** (Figure 3A). This new compound was also able to inhibit autophosphorylation of GST-RIP1 in the in-vitro kinase assay (Figure 3B), similar to the fluorescent Nec-1 analog. Similar to **20**, compound **26** also displayed excitation/emission maxima at 495 and 515 nm, respectively, and robust signal to background ratios were observed under the assay conditions (Figure S2).

K_D determination of fluorescent-Nec analogs in FP assay

To test the binding capabilities of **20** and **26** in FP assays, the GST-RIP1 kinase domain protein was titrated into 50 nM **20** and 50 nM **26** (Figure 4). In both cases, we observed a dose-dependent increase in polarization indicative of binding. We fit the curves to determine K_D values for compounds **20** (2.6 ± 0.3 μM) and **26** (3.4 ± 0.5 μM). These low micromolar K_D values are in good concert with somewhat reduced activity of fluorescent analogs observed in ^{32}P assays when compared to parental Nec-1 and Nec-3 (Figures 2D and 3B), which display sub-micromolar activities in the cell based assays [10].

Competitive binding experiments using FP assay

To ensure that the binding of **20** is specific and reversible, we performed competition assays with the Nec-1 intermediate analogs, **4**, **5**, and **6** (Figure 5A). As expected, these compounds were able to compete with **20** with comparable K_i values (Table 1) to the 2.6 ± 0.3 μM K_D for **20**. The rank order of the K_i values of the intermediate analogs was the same as their activities in a cell viability assay (Figure 2B). Therefore, we continued our characterization by testing **20** in competition assays with **1**, **Rac-3**, the optimized R-enantiomer (**R-3**), and inactive compound **2** (Figure 5B). **Rac-3**, **R-3**, **1** were able to displace **20** from GST-RIP1 with the rank order of **R-3**, **Rac-3**, **1** (Table 1) the same as we saw in the cell based SAR study [15]. The inactive analog did not compete with **20** demonstrating the specificity of this assay. Overall, these data confirm that we are measuring specific binding of Nec-1 to RIP1 kinase and the competition assays reflect the affinities of Nec-1 analogs to RIP1 kinase.

Since **20** is specific and reversible in binding to GST-RIP1, we tried cross-competition titrations with Nec-3 (**7**) and Nec-4 (**9**) to understand if there are differences in the binding mode of these structurally different necrostatins. Both compounds **7** and **9** are able to compete with **20** for binding to GST-RIP1 (Figure 5C). At the same time, differences, albeit subtle, could also be detected. Compound **9** is a slightly better competitor than **7** with a lower K_i value (Table 1) that is similar to **R-3**. Although **7** displayed similar potency to **Rac-3** in the cell viability assay (Figure 2B), **7** was a modestly weaker competitor with **20** in the FP assay. Our previous data suggests that Nec-1 is ATP competitive [10] and docks into the ATP binding pocket of the DLG-out conformation of RIP1 (Figure 1B). Therefore, the cross-competition data revealed that even though Nec-1 and Nec-4 are structurally very different, these molecules share overlapping binding sites. It is probable that Nec-3 is also binding close to the ATP binding site but at a region somewhat distal to Nec-1.

We also tested compound **26** for specificity by conducting competition titrations with Nec-3 (**7**) and its inactive analog, Nec-3i (**8**) [10] (Figure 5D). As seen with compound **20**, **7** is able to compete with **26** for binding to GST-RIP1, while **8** does not compete. As with **20**, **26** displayed a moderately decreased binding affinity for GST-RIP1 compared to the parental

compound (0.76 ± 0.21 μM K_i of **7** versus 3.4 ± 0.5 μM K_D of **26**), likely indicating some hindrance from the linker/fluorescein groups. We also tested **26** in cross-competition assays with **Rac-3** and **9** (Figure 5E). Compound **9** was again a slightly better competitor than **Rac-3** with K_i and IC_{50} values comparable to **7** (Table 2). Overall, all three compounds cross-compete with each other but compound **9** is able to more effectively displace both **20** and **26** in comparison to the parent compounds **Rac-3** and **7**, respectively. This suggests that Nec-4 binding likely significantly overlaps with both the Nec-1 and the Nec-3 binding sites. Conversely, since Nec-1 and Nec-3 compete less strongly with each other, they may only have moderate overlap in binding sites. Altogether, these results establish a new FP based necrostatin/RIP1 assay, which provides a rapid and robust method for comparing binding modes of different classes of RIP1 kinase inhibitors.

To further understand the binding sites of the different necrostatins, we pursued more docking studies with RIP1. The induced fit docking of **3** demonstrated a strong preference for the DLG-out conformation. This conformation places the indole of **3** in the pocket where the adenine of ATP likely binds and the hydantoin is positioned between the hinge and the N-terminal domain/P-loop (Figure 1B, S3A). We generated a ligand interaction diagram to further understand the nature of the Nec-1 binding pocket (Figure S3B). The pocket has both hydrophobic character and a key hydrogen bond that is typically found in active site kinase inhibitors [47]. Additional docking studies with **7** revealed that Nec-3 could dock into both DLG conformations in a similar manner but prefers the DLG-in form. To compare to the Nec-1 binding site we used the DLG-out docking and discovered that compound **7** makes significant contacts with the hinge and C-terminal domain immediately following the hinge (Figure S4). This conformation of **7** would position the fluorescein group of **26** out towards solvent near the C-terminal domain. The nature of the pocket is predominately hydrophobic with the potential for form stacking interactions. Placing both **3** and **7** together in the DLG-out conformation indicates that they have different but partially overlapping binding sites (Figure 6B). The fused benzene ring portion of **7** binds to the same region as the hydantoin of **3** but has no significant overlap with the indole. This is in agreement with our FP competition results, which indicated that **3** and **7** compete with each other weakly likely due to partially overlapping binding sites. Compound **9** also docked in both DLG-out and DLG-in conformations of RIP1 but to understand the competitions with **3** and **7**, we used the DLG-out docking. The docking revealed that **9** contacts both the adenine binding pocket and the hinge (Figure S5). The interactions in the pocket are mostly hydrophobic but also involve two hydrogen bonds. This binding orientation would disrupt hydantoin binding of **3** and potentially cause steric clashes with the indole ring (Figure 6C). Compound **9** binds in a similar manner as **7** with all interaction being disrupted except for the pendent methoxyphenyl (Figure 6D). These docking studies support our results from the FP competition studies where **9** competes strongly with both **3** and **7**, while **3** and **7** compete but to a lesser degree.

Feasibility of FP assay for HTS

In order to validate the use of both **20** and **26** for HTS FP assays, we performed DMSO tolerance and Z'-score analysis. DMSO is a solvent generally used to dissolve small molecules used in screening assays. Therefore, we tested our FP assay to determine the usable range of DMSO, which itself does not have an effect on the polarization of either **20** or **26** (Figure 7A,C). Binding of both fluorescent molecules to GST-RIP1 was reduced by <30% at DMSO concentrations of up to 5%, establishing the tolerated range for DMSO between 0 and 5%.

We further analyzed compounds **20** and **26** in Z'-score analysis. In this case we used the fluorescent compound/GST-RIP1 as the positive control and the fluorescent compound/

GST-RIP1/non-fluorescent parent compound as the negative control. For compound **20** Z' is 0.62, while for compound **26** Z' is 0.57 (Figure 7B,D). Both of these compounds are well suited for future use in HTS-FP assays for the identification and development of RIP1 inhibitors.

In summary, we have identified new directions for Nec-1 and Nec-3 modification and developed two fluorescein-labeled necrostatins that specifically and reversibly bind to RIP1. Both of these molecules are well suited for use in HTS-FP assays, providing a simple and robust homogeneous assay for the identification of new RIP1 inhibitors. We also discovered that Nec-1 (**3**), Nec-3 (**7**), and Nec-4 (**9**) are able to cross-compete with each but to varying degrees. First, these data along with our docking studies indicate that all three structurally distinct necrostatins interact with the active center of RIP1 kinase through overlapping binding sites. Second, Nec-4 is able to effectively compete with both Nec-1 and Nec-3 and our docking results are consistent with the model in which Nec-4 binding site overlaps with both Nec-1 and Nec-3. On the other hand, Nec-1 and Nec-3 occupy more distinct, less overlapping binding sites. Further structural studies are required to characterize the conformations of RIP1 kinase preferred by Nec-3 and Nec-4 as our docking analysis suggested that these molecules may interact with both DLG-out and DLG-in conformations. This will define whether these molecules are acting as allosteric inhibitors in a binding mode different from Nec-1. Furthermore, our data suggest that using both fluorescent-Nec-1 and fluorescent-Nec-3 in primary or secondary assays will provide a simple and robust method to assess RIP1 binding modes of new molecules allowing for the selection of molecules distinct from the currently available classes of necrostatins.

Supplementary Material

Refer to Web version on PubMed Central for supplementary material.

Acknowledgments

We thank Albert Tai and the Study Center on the Immunogenetics of Infectious Disease (SCIID) at Tufts University for use of the nanodrop instrument and SpectraMax M5 plate reader. This work was supported by a grant from the NIGMS/NIH to A.D. (GM084205) and the Harvard NeuroDiscovery Center (HNDC).

References

1. Dunai Z, Bauer PI, Mihalik R. Necroptosis: Biochemical, Physiological and Pathological Aspects. Pathol. Oncol. Res. 2011
2. Galluzzi L, Vanden Berghe T, Vanlangenakker N, Buettner S, Eisenberg T, Vandenabeele P, Madeo F, Kroemer G. Programmed necrosis from molecules to health and disease. Int. Rev. Cell Mol. Biol. 2011; 289:1–35. [PubMed: 21749897]
3. Cho YS, Challa S, Moquin D, Genga R, Ray TD, Guildford M, Chan FK. Phosphorylation-driven assembly of the RIP1-RIP3 complex regulates programmed necrosis and virus-induced inflammation. Cell. 2009; 137:1112–1123. [PubMed: 19524513]
4. Zhang DW, Shao J, Lin J, Zhang N, Lu BJ, Lin SC, Dong MQ, Han J. RIP3, an energy metabolism regulator that switches TNF-induced cell death from apoptosis to necrosis. Science. 2009; 325:332–336. [PubMed: 19498109]
5. He S, Wang L, Miao L, Wang T, Du F, Zhao L, Wang X. Receptor interacting protein kinase-3 determines cellular necrotic response to TNF-alpha. Cell. 2009; 137:1100–1111. [PubMed: 19524512]
6. Christofferson DE, Yuan J. Necroptosis as an alternative form of programmed cell death. Curr. Opin. Cell Biol. 2010; 22:263–268. [PubMed: 20045303]
7. Vandenabeele P, Galluzzi L, Vanden Berghe T, Kroemer G. Molecular mechanisms of necroptosis: an ordered cellular explosion. Nat. Rev. Mol. Cell Biol. 2010; 11:700–714. [PubMed: 20823910]

8. Vandenabeele P, Declercq W, Van Herreweghe F, Vanden Berghe T. The role of the kinases RIP1 and RIP3 in TNF-induced necrosis. Science signaling. 2010; 3:re4. [PubMed: 20354226]
9. Sun X, Yin J, Starovasnik MA, Fairbrother WJ, Dixit VM. Identification of a novel homotypic interaction motif required for the phosphorylation of receptor-interacting protein (RIP) by RIP3. J. Biol. Chem. 2002; 277:9505–9511. [PubMed: 11734559]
10. Degterev A, Hitomi J, Germscheid M, Ch'en IL, Korkina O, Teng X, Abbott D, Cuny GD, Yuan C, Wagner G, Hedrick SM, Gerber SA, Lugovskoy A, Yuan J. Identification of RIP1 kinase as a specific cellular target of necrostatins. Nat. Chem. Biol. 2008; 4:313–321. [PubMed: 18408713]
11. Bertrand MJ, Vandenabeele P. The Ripoptosome: death decision in the cytosol. Molecular cell. 2011; 43:323–325. [PubMed: 21816342]
12. Teng X, Keys H, Jeevanandam A, Porco JA Jr, Degterev A, Yuan J, Cuny GD. Structure-activity relationship study of [1,2,3]thiadiazole necroptosis inhibitors. Bioorg. Med. Chem. Lett. 2007; 17:6836–6840. [PubMed: 17964153]
13. Jagtap PG, Degterev A, Choi S, Keys H, Yuan J, Cuny GD. Structure-activity relationship study of tricyclic necroptosis inhibitors. J. Med. Chem. 2007; 50:1886–1895. [PubMed: 17361994]
14. Degterev A, Huang Z, Boyce M, Li Y, Jagtap P, Mizushima N, Cuny GD, Mitchison TJ, Moskowitz MA, Yuan J. Chemical inhibitor of nonapoptotic cell death with therapeutic potential for ischemic brain injury. Nat. Chem. Biol. 2005; 1:112–119. [PubMed: 16408008]
15. Teng X, Degterev A, Jagtap P, Xing X, Choi S, Denu R, Yuan J, Cuny GD. Structure-activity relationship study of novel necroptosis inhibitors. Bioorg. Med. Chem. Lett. 2005; 15:5039–5044. [PubMed: 16153840]
16. Degterev A, Yuan J. Expansion and evolution of cell death programmes. Nat. Rev. Mol. Cell Biol. 2008; 9:378–390. [PubMed: 18414491]
17. Sherman W, Day T, Jacobson MP, Friesner RA, Farid R. Novel procedure for modeling ligand/receptor induced fit effects. J Med Chem. 2006; 49:534–553. [PubMed: 16420040]
18. Friesner RA, Banks JL, Murphy RB, Halgren TA, Klicic JJ, Mainz DT, Repasky MP, Knoll EH, Shelley M, Perry JK, Shaw DE, Francis P, Shenkin PS. Glide: a new approach for rapid, accurate docking and scoring. 1. Method and assessment of docking accuracy. J Med Chem. 2004; 47:1739–1749. [PubMed: 15027865]
19. Halgren TA, Murphy RB, Friesner RA, Beard HS, Frye LL, Pollard WT, Banks JL. Glide: a new approach for rapid, accurate docking and scoring. 2 Enrichment factors in database screening. J Med Chem. 2004; 47:1750–1759. [PubMed: 15027866]
20. Eswar N, John B, Mirkovic N, Fiser A, Ilyin VA, Pieper U, Stuart AC, Marti-Renom MA, Madhusudhan MS, Yerkovich B, Sali A. Tools for comparative protein structure modeling and analysis. Nucleic Acids Res. 2003; 31:3375–3380. [PubMed: 12824331]
21. Pieper U, Eswar N, Braberg H, Madhusudhan MS, Davis FP, Stuart AC, Mirkovic N, Rossi A, Marti-Renom MA, Fiser A, Webb B, Greenblatt D, Huang CC, Ferrin TE, Sali A. MODBASE, a database of annotated comparative protein structure models, and associated resources. Nucleic Acids Res. 2004; 32:D217–D222. [PubMed: 14681398]
22. Sanchez R, Sali A. Evaluation of comparative protein structure modeling by MODELLER-3. Proteins Suppl. 1997; 1:50–58.
23. Laskowski RA, Rullmannn JA, MacArthur MW, Kaptein R, Thornton JM. AQUA and PROCHECK-NMR: programs for checking the quality of protein structures solved by NMR. J Biomol NMR. 1996; 8:477–486. [PubMed: 9008363]
24. Potterton E, Briggs P, Turkenburg M, Dodson E. A graphical user interface to the CCP4 program suite. Acta Crystallogr D Biol Crystallogr. 2003; 59:1131–1137. [PubMed: 12832755]
25. Hooft RW, Vriend G, Sander C, Abola EE. Errors in protein structures. Nature. 1996; 381:272. [PubMed: 8692262]
26. Vaguine AA, Richelle J, Wodak SJ. SFCHECK: a unified set of procedures for evaluating the quality of macromolecular structure-factor data and their agreement with the atomic model. Acta Crystallogr D Biol Crystallogr. 1999; 55:191–205. [PubMed: 10089410]
27. Rossi KA, Weigelt CA, Nayeem A, Krystek SR Jr. Loopholes and missing links in protein modeling. Protein Sci. 2007; 16:1999–2012. [PubMed: 17660258]

28. Xiang Z, Soto CS, Honig B. Evaluating conformational free energies: the colony energy and its application to the problem of loop prediction. Proc Natl Acad Sci U S A. 2002; 99:7432–7437. [PubMed: 12032300]
29. Shan Y, Kim ET, Eastwood MP, Dror RO, Seeliger MA, Shaw DE. How does a drug molecule find its target binding site? J Am Chem Soc. 2011; 133:9181–9183. [PubMed: 21545110]
30. Shaw DE, Maragakis P, Lindorff-Larsen K, Piana S, Dror RO, Eastwood MP, Bank JA, Jumper JM, Salmon JK, Shan Y, Wriggers W. Atomic-level characterization of the structural dynamics of proteins. Science. 2010; 330:341–346. [PubMed: 20947758]
31. Guvench O, MacKerell AD Jr. Comparison of protein force fields for molecular dynamics simulations. Methods Mol Biol. 2008; 443:63–88. [PubMed: 18446282]
32. Burgey CS, Robinson KA, Lyle TA, Sanderson PE, Lewis SD, Lucas BJ, Krueger JA, Singh R, Miller-Stein C, White RB, Wong B, Lyle EA, Williams PD, Coburn CA, Dorsey BD, Barrow JC, Stranieri MT, Holahan MA, Sitko GR, Cook JJ, McMasters DR, McDonough CM, Sanders WM, Wallace AA, Clayton FC, Bohn D, Leonard YM, Detwiler TJ Jr, Lynch JJ Jr, Yan Y, Chen Z, Kuo L, Gardell SJ, Shafer JA, Vacca JP. Metabolism-directed optimization of 3-aminopyrazinone acetamide thrombin inhibitors. Development of an orally bioavailable series containing P1 and P3 pyridines. Journal of medicinal chemistry. 2003; 46:461–473. [PubMed: 12570369]
33. Marchand P, Antoine M, Le Baut G, Czech M, Baasner S, Gunther E. Synthesis and structure-activity relationships of N-aryl(indol-3-yl)glyoxamides as antitumor agents. Bioorganic & medicinal chemistry. 2009; 17:6715–6727. [PubMed: 19682911]
34. Zhu X, Ge Y. Synthesis of chloro-substituted indole-3-acetonitriles. Huaxue Shiji. 2008; 30:161.
35. Nikolovska-Coleska Z, Wang R, Fang X, Pan H, Tomita Y, Li P, Roller PP, Krajewski K, Saito NG, Stuckey JA, Wang S. Development and optimization of a binding assay for the XIAP BIR3 domain using fluorescence polarization. Anal. Biochem. 2004; 332:261–273. [PubMed: 15325294]
36. Zhang JH, Chung TD, Oldenburg KR. A Simple Statistical Parameter for Use in Evaluation and Validation of High Throughput Screening Assays. J. Biomol. Screen. 1999; 4:67–73. [PubMed: 10838414]
37. Xiao Y, Li H, Zhang J, Volk A, Zhang S, Wei W, Breslin P. TNF-{alpha}/Fas-RIP-1-induced cell death signaling separates murine hematopoietic stem cells/progenitors into two distinct populations. Blood. 2011
38. Yamanaka K, Saito Y, Yamamori T, Urano Y, Noguchi. 24(S)-hydroxycholesterol induces neuronal cell death through necroptosis, a form of programmed necrosis. J. Biol. Biol. Chem. 2011; 286:24666–24673.
39. Sawai H, Domae N. Discrimination between primary necrosis and apoptosis by necrostatin-1 in Annexin V-positive/propidium iodide-negative cells. Biochem. Biophys. Res. Commun. 2011; 411:569–573. [PubMed: 21763280]
40. Davis CW, Hawkins BJ, Ramasamy S, Irrinki KM, Cameron BA, Islam K, Daswani VP, Doonan PJ, Manevich Y, Madesh M. Nitration of the mitochondrial complex I subunit NDUFB8 elicits RIP1- and RIP3-mediated necrosis. Free Radic. Biol. Med. 2010; 48:306–317. [PubMed: 19897030]
41. Lim SY, Davidson SM, Mocanu MM, Yellon DM, Smith CC. The cardioprotective effect of necrostatin requires the cyclophilin-D component of the mitochondrial permeability transition pore. Cardiovasc. Drugs Ther. 2007; 21:467–469. [PubMed: 17965927]
42. Trichonas G, Murakami Y, Thanos A, Morizane Y, Kayama M, Debouck CM, Hisatomi T, Miller JW, Vavvas DG. Receptor interacting protein kinases mediate retinal detachment-induced photoreceptor necrosis and compensate for inhibition of apoptosis. Proc. Natl. Acad. Sci. U.S.A. 2010; 107:21695–21700. [PubMed: 21098270]
43. Xu X, Chua KW, Chua CC, Liu CF, Hamdy RC, Chua BH. Synergistic protective effects of humanin and necrostatin-1 on hypoxia and ischemia/reperfusion injury. Brain Res. 2010; 1355:189–194. [PubMed: 20682300]
44. You Z, Savitz SI, Yang J, Degterev A, Yuan J, Cuny GD, Moskowitz MA, Whalen MJ. Necrostatin-1 reduces histopathology and improves functional outcome after controlled cortical impact in mice. J. Cereb. Blood Flow Metab. 2008; 28:1564–1573. [PubMed: 18493258]

45. Zhu S, Zhang Y, Bai G, Li H. Necrostatin-1 ameliorates symptoms in R6/2 transgenic mouse model of Huntington's disease. Cell Death Dis. 2011; 2:e115. [PubMed: 21359116]

46. McNeal SI, LeGolvan MP, Chung CS, Ayala A. The dual functions of receptor interacting protein 1 in fas-induced hepatocyte death during sepsis. Shock. 2011; 35:499–505. [PubMed: 21263386]

47. Noble ME, Endicott JA, Johnson LN. Protein kinase inhibitors: insights into drug design from structure. Science. 2004; 303:1800–1805. [PubMed: 15031492]

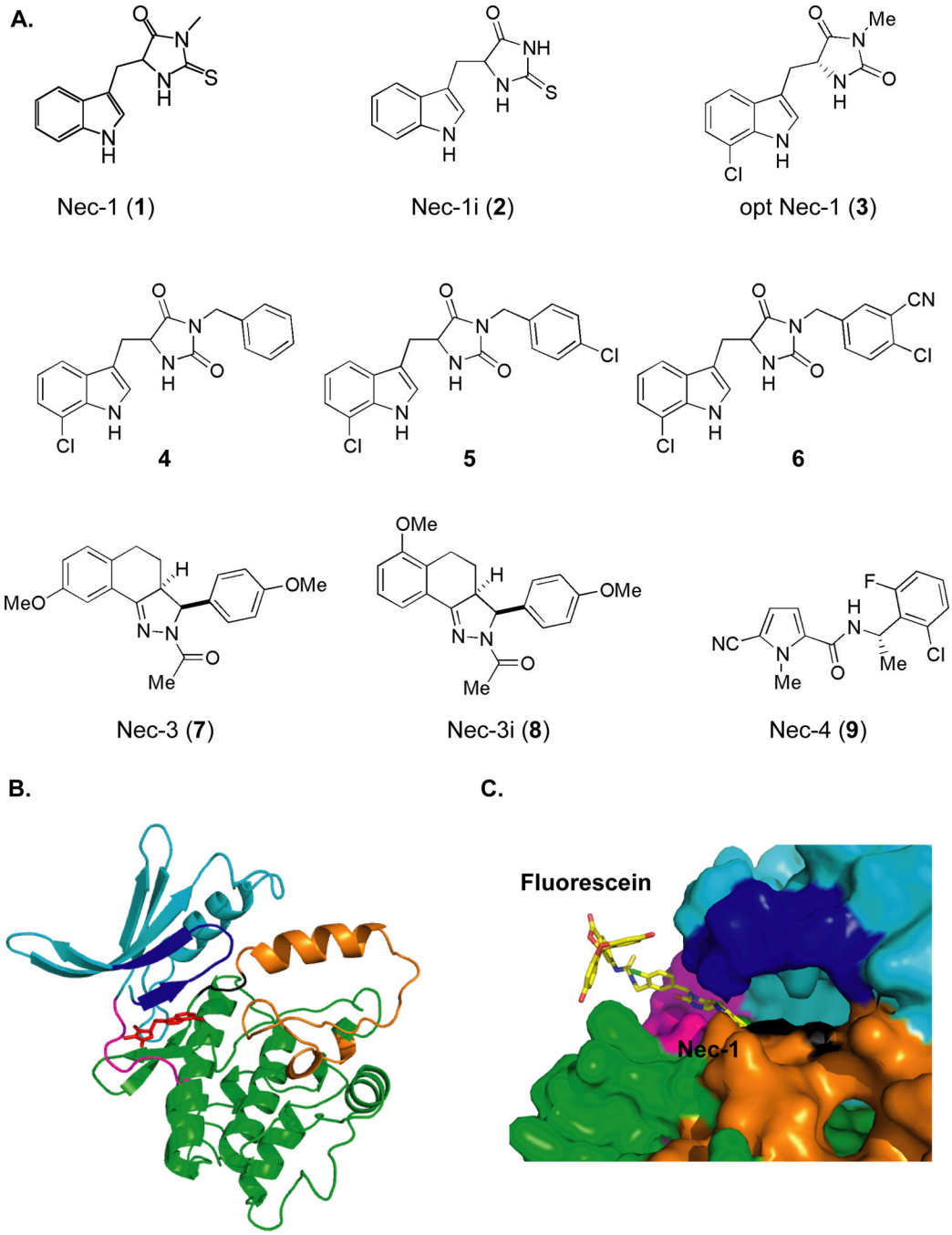

Figure 1.

(A) Structures of the different necrostatins. (B) Induced fit docking model of Nec-1-RIP1. Nec-1 (**3**) was docked into the molecular model of RIP1 kinase domain (aa 22–291) as described in the Materials and Methods. RIP1 is shown as a cartoon with the N-terminal domain in cyan, P-loop in blue, hinge in magenta, DLG in black, activation segment in orange, and C-terminal domain in green with **3** shown as sticks in red. (C) A surface representation zoomed in to the ATP-binding region of RIP1 is shown with Nec-1 and fluorescein portions of **20** labeled. Different views of this complex are shown in Figure S1. The model of RIP1/**20** complex indicates that fluorescein does not interact with RIP1. RIP1

is color-coded as described in B and **20** is color-coded by element: carbon in yellow, nitrogen in blue, and oxygen in red. Images were made using PyMol.

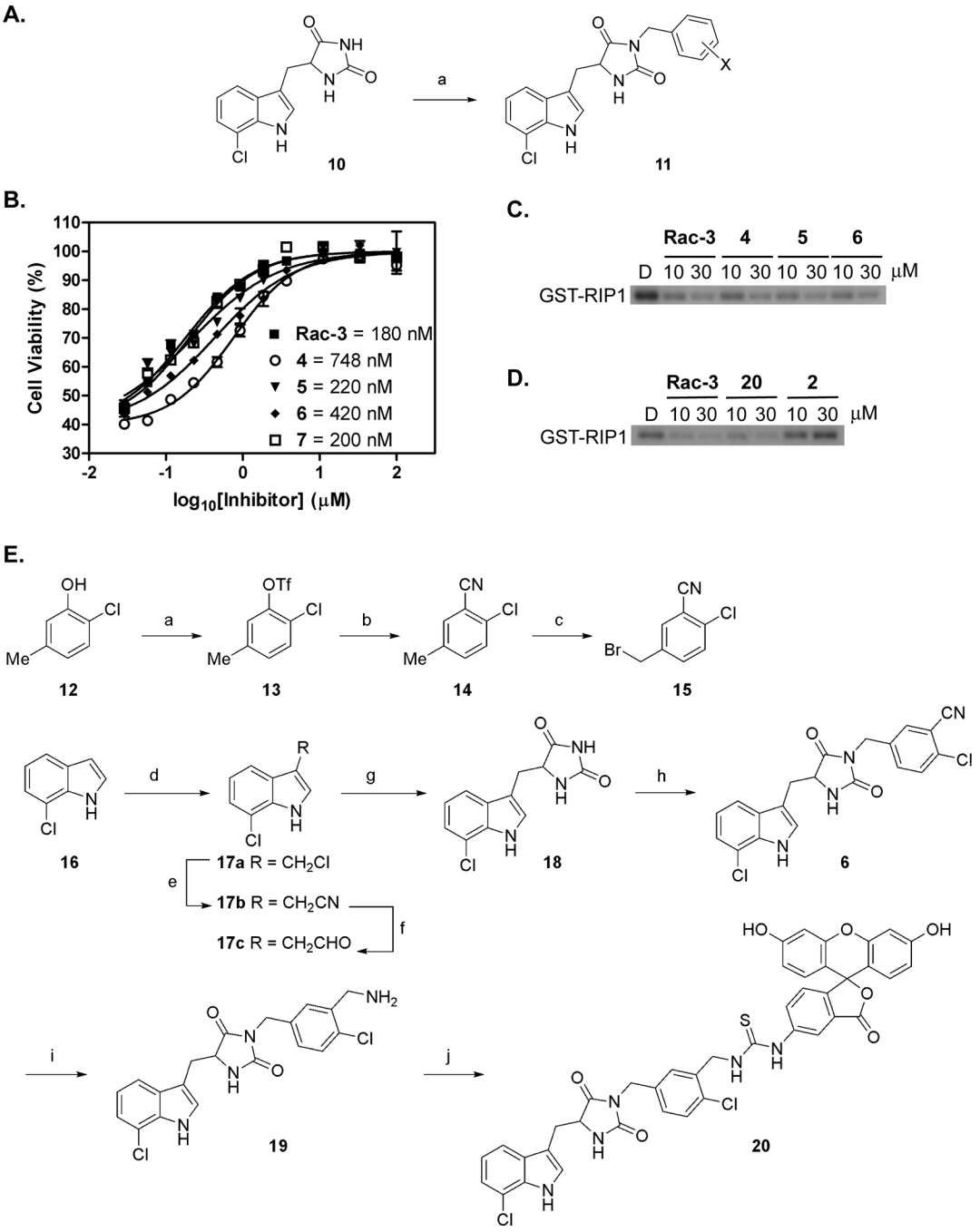

Figure 2.

(A) Synthesis of Nec-1 derivatives **4**, **5**, and **6**. Compound **10** was made as previously described [15]. a) various benzyl bromide, KOH, EtOH/H_2O, 95°C, 14h. (B) The dose-response curves of optimized racemic Nec-1 (**Rac-3**), intermediate analogs (**4**, **5**, **6**), and Nec-3 (**7**) in a necroptosis cell-based assay as previously described [14] [15]. Viability was normalized to cells treated with DMSO. (C) In vitro kinase assay of Nec-1 intermediate analogs. The autophosphorylation of recombinant GST-RIP1 was performed as indicated in the Materials and Methods. Samples were run on SDS-PAGE gel and autophosphorylation was visualized by autoradiography. D is the DMSO control sample while the concentrations

of Nec-1 analogs are shown above the gel. (D) In vitro kinase assay with the **Rac-3**, **20**, and inactive Nec-1 (**2**). Compound **20** is able to inhibit the autophosphorylation activity of GST-RIP1. (E) Synthesis of Nec-1 fluorescein derivative. a) triflic anhydride, Py, CH_2Cl_2, 0°C, 6h; b) $Zn(CN)_2$, $Pd(PPh_3)_4$, DMF, 60°C, 14h; c) NBS, AIBN, CCl4, reflux, 12h; d) N,N-dimethylmethylene ammonium chloride, CH_2Cl_2, rt, 2h, then 1M NaOH; e) NaCN, EtOAc, DMSO, 80°C, 6h; f) DIBAL, toluene, −78°C to rt, 2h; g) $(NH_4)_2CO_3$, KCN, EtOH, H_2O, 60°C, 14h; h) **15**, KOH, EtOH/H_2O, 95°C, 8h; i) H_2, Raney Ni, NH_3 in MeOH, 6h; j) fluorescein isothiocyanate (FITC), DMF, 0°C to rt, 1h.

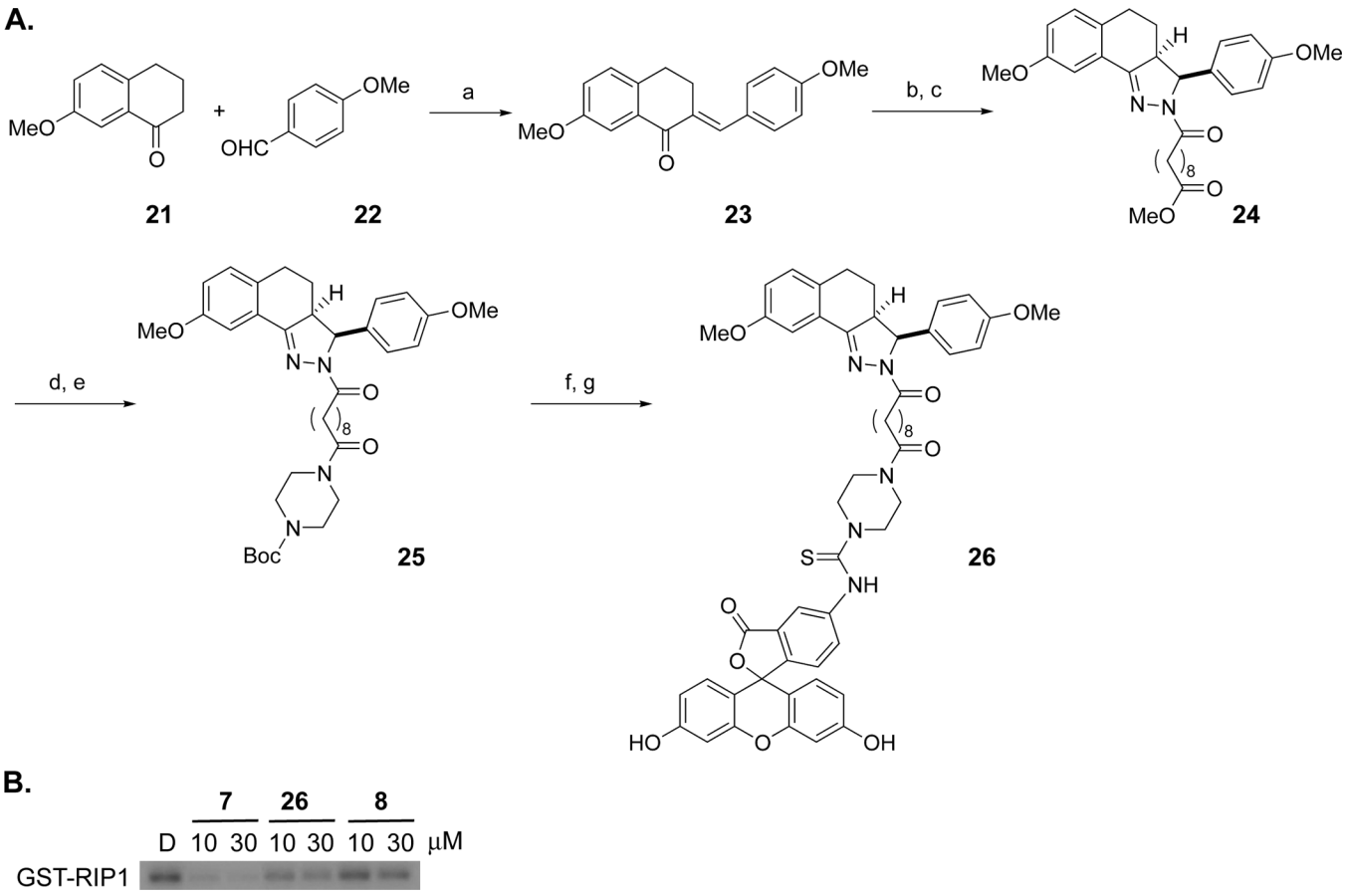

Figure 3.

(A) Synthesis of Nec-3 fluorescein derivative. a) NaOH, EtOH, H_2O, rt, 2h; b) $(CH_3)_3CCOOH$, hydrazine hydrate, EtOH, 120°C, reflux, 16h; c) Methyl 10-chloro-10-oxodecanoate, sat. aq. $NaHCO_3$, EtOAc, 2h; d) NaOH, MeOH, 6h; e) N-Boc-piperazine, HBTU, DIPEA, CH_2Cl_2, rt, 14h; f) TFA, CH_2Cl_2, rt, 1h; g) FITC, DMF, 0°C to rt, 1h. (B) In vitro kinase assay with the Nec-3 (**7**), fluorescein-Nec-3 (**26**), and inactive Nec-3 (**8**). Compound **26** is able to inhibit the autophosphorylation activity of GST-RIP1.

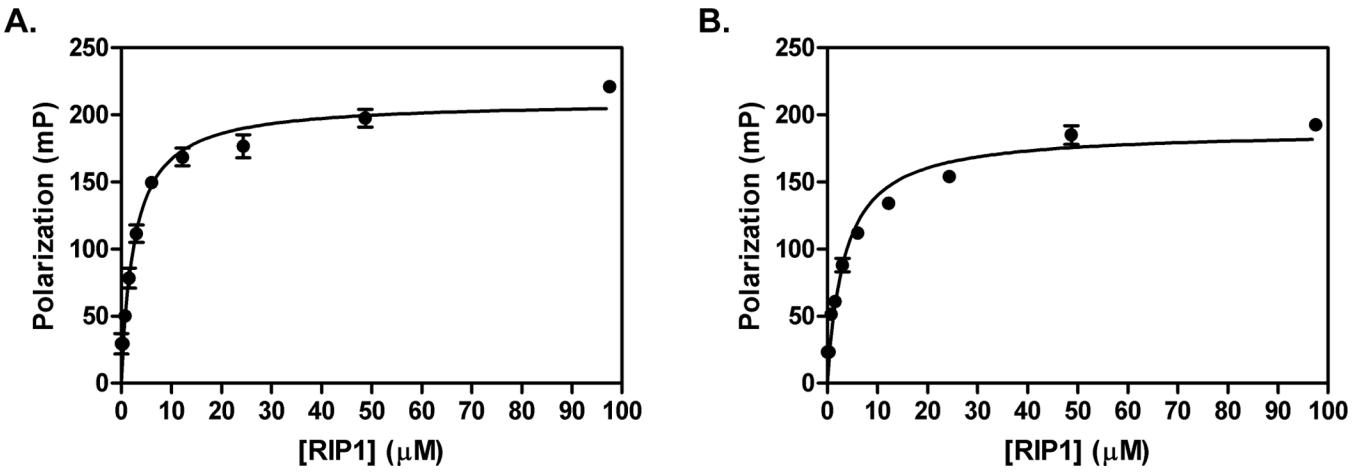

Figure 4.

K_D determination of fluorescent analogs. (A) Increasing concentrations of GST-RIP1 protein were titrated into **20** and the curve was fitted to obtain a K_D of 2.6 ± 0.3 μM with a R^2 value of 0.96 and B_{max} value of 210 mP. (B) Increasing concentrations of GST-RIP1 protein were titrated into **26** and the curve was fitted to obtain a K_D of 3.4 ± 0.5 μM with a R^2 value of 0.96 and B_{max} value of 188 mP.

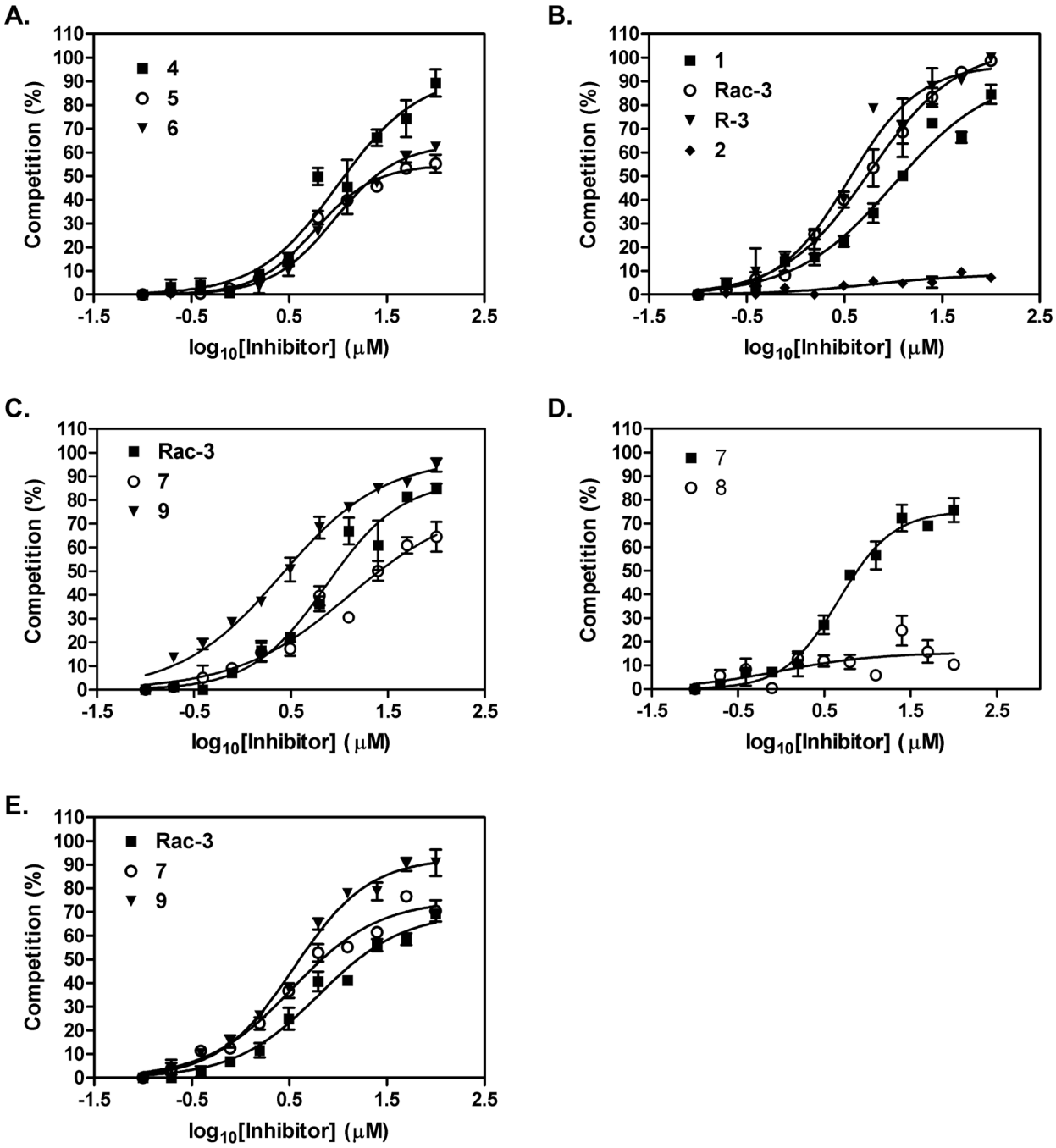

Figure 5.

Competition Assays with fluorescent analogs. (A) GST-RIP1 and **20** were incubated together for five minutes and then increasing concentrations of **4**, **5**, and **6** were titrated. Curves were fit to determine IC_{50} and K_i values for each compound (Table 1 and 2). (B) Competition assays with GST-RIP1/**20** and **1**, **2**, **Rac-3**, and **R-3**. (C) Competition assays with GST-RIP1/**20** and **Rac-3**, **7**, and **9**. (D) Competition assays with GST-RIP1/**26** and **7** and **8**. (E) Competition assays with GST-RIP1/**26** and **Rac-3**, **7**, and **9**.

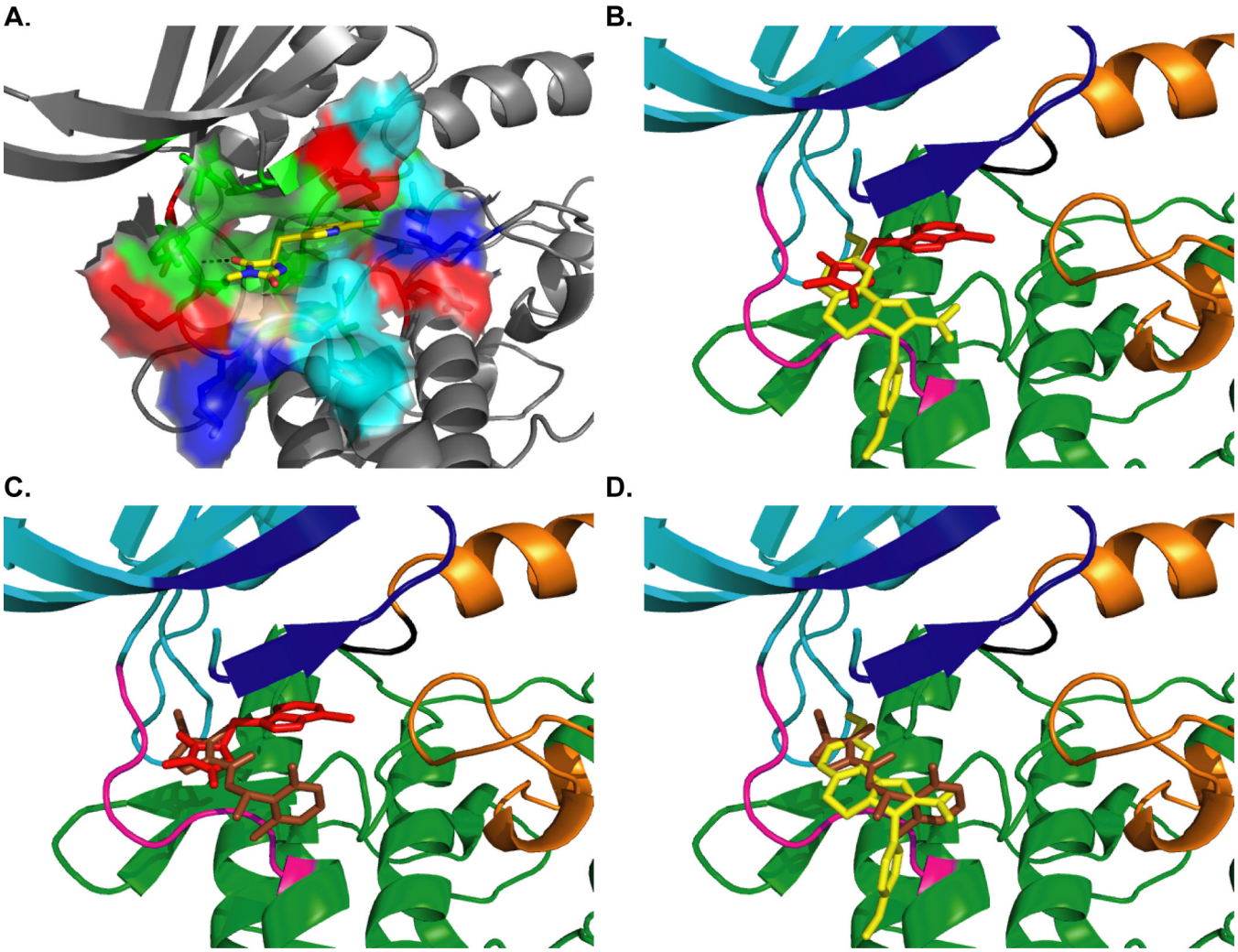

Figure 6.

Docking of the necrostatins to RIP1. (A) The induced fit docking model of Nec-1, color-coded as in Figure 1C, and RIP1 is shown. The residues making the binding pocket for Nec-1 determined from ligand interaction diagram (Figure S2) are color-coded by amino acid type: green-hydrophobic, cyan-polar, red-acidic, blue-basic, and glycinetan. The black dashed line indicates a hydrogen bond. (B) Nec-1 (**3**) in red and Nec-3 (**7**) in yellow are docked into the DLG out conformation of RIP1. The two molecules partially overlap in their binding sites. (C) Nec-1 (**3**) in red and Nec-4 (**9**) in brown docked into the DLG out conformation of RIP1. The two molecules partially overlap. (D) Nec-3 (**7**) in yellow and Nec-4 (**9**) in brown are docked into the DLG out conformation of RIP1. The two molecules significantly overlap with each other.

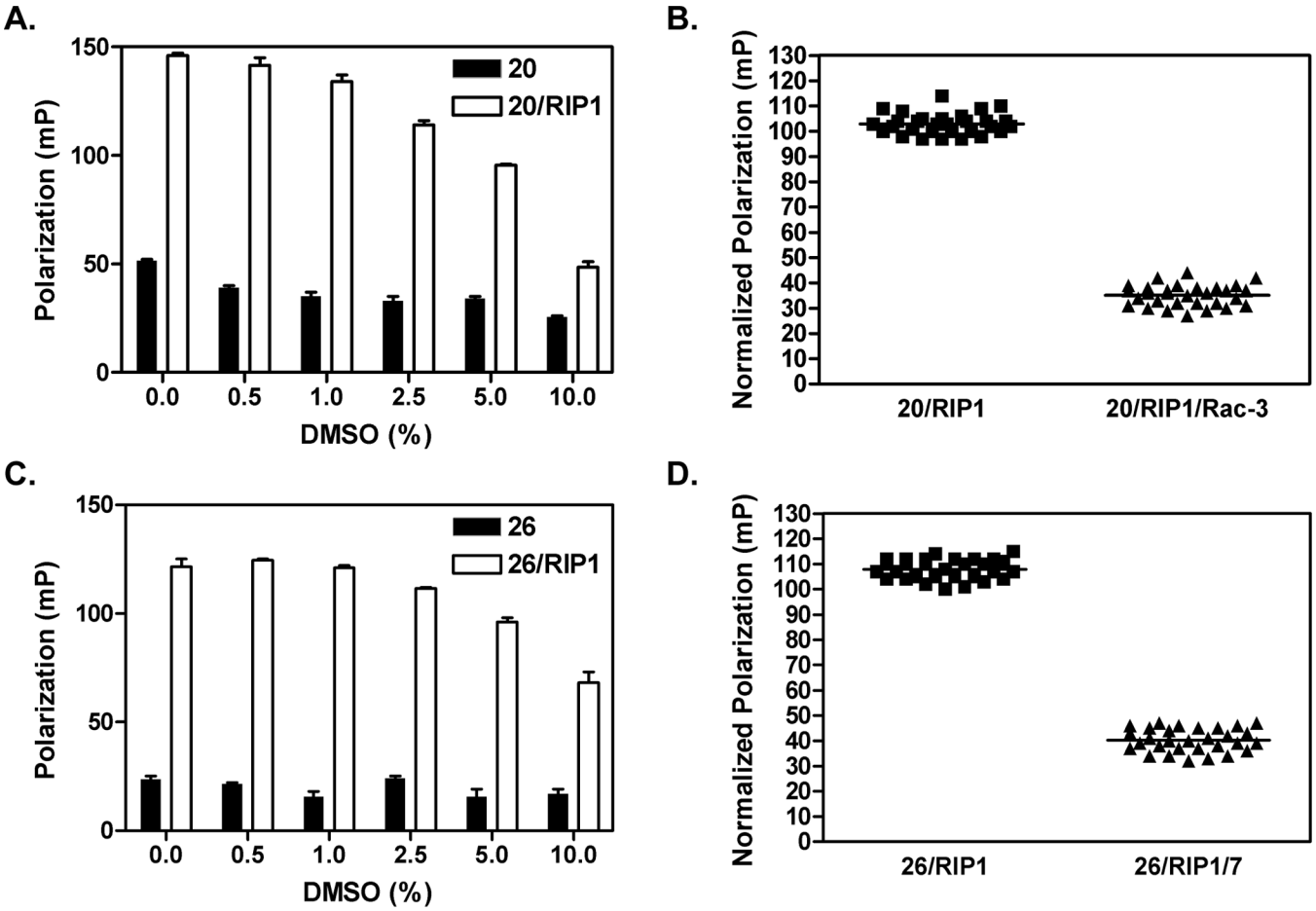

Figure 7.

Feasibility of FP assay for HTS. (A) DMSO tolerance of **20** in FP was tested with **20** alone (black bars) and GST-RIP1/**20** complex (white bars) in 0–10% DMSO. Concentrations at or below 5% are well-tolerated in this assay. (B) Z'-score for **20** was tested in three separate experiments in 10-wells each with GST-RIP1/**20** and GST-RIP1/**20**/**Rac-3**. The average from all 30 wells was used to normalize each of the three separate experiments. Z' is 0.62 demonstrating that this is an excellent assay for HTS. (C) Same as in (A) except using **26**. (D) Z'-score for **26** was tested as described in (B) with GST-RIP1/**26** and GST-RIP1/**26**/**7**. Z' is 0.57 demonstrating that this is an excellent assay for HTS.

Table I

Summary of Competition Assays with 20

Compound	IC_{50} (μM)	K_i (μM)
4	8.5 ± 1.2	3.4 ± 0.6
5	6.0 ± 0.2	2.1 ± 0.1
6	9.6 ± 0.6	3.9 ± 0.3
1	9.9 ± 0.6	4.1 ± 0.3
R-3	3.6 ± 0.7	0.92 ± 0.36
Rac-3	5.7 ± 1.0	2.0 ± 0.5
7	10.7 ± 1.8	4.5 ± 0.9
9	2.6 ± 0.1	0.46 ± 0.05

Table 2

Summary of Competition Assays with 26

Compound	IC_{50} (μM)	K_i (μM)
7	3.9 ± 0.7	0.76 ± 0.21
1	7.0 ± 0.7	2.4 ± 0.4
9	3.9 ± 0.5	0.80 ± 0.27